# An apparatus and methodology for high-power SQUID-detected ferromagnetic resonance measurements

J. M. O'Reilly (iD), and P. Stamenov (iD)

View Online          Export Citation          CrossMark

### ARTICLES YOU MAY BE INTERESTED IN

SQUID-detected FMR: Resonance in single crystalline and polycrystalline yttrium iron garnet
Review of Scientific Instruments **89**, 044701 (2018); https://doi.org/10.1063/1.5009731

Guided wave phased array sensor based on a Galfenol flake-epoxy composite patch with unique circular comb pattern
AIP Advances **9**, 035022 (2019); https://doi.org/10.1063/1.5080143

Magnetic properties of permalloy antidot array fabricated by interference lithography
AIP Advances **9**, 035136 (2019); https://doi.org/10.1063/1.5080111

# An apparatus and methodology for high-power SQUID-detected ferromagnetic resonance measurements

View Online    Export Citation    CrossMark

J. M. O'Reilly[a] (iD) and P. Stamenov[b] (iD)

## AFFILIATIONS

School of Physics, Centre for Research on Adaptive Nanostructures and Nanodevices (CRANN) and Advanced Materials
Bio-Engineering Research Centre (AMBER), Trinity College, Dublin 2, Ireland

**Note:** This paper was presented at the 2019 Joint MMM-Intermag Conference.
[a] Electronic mail: oreillj5@tcd.ie
[b] Electronic mail: stamenop@tcd.ie

## ABSTRACT

Historically, ferromagnetic resonance has been dominated by inductive techniques, for the best part of the last 80 years. It has been only in the last 20 years that non-inductive techniques, such as Ferromagnetic Resonance Force Microscopy (FMRFM) and Magneto-optical Kerr Effect (MOKE), have been used to study, for example, the spatial distribution of resonance modes. Neither of these techniques is absolute - i.e. provides information on the amplitude of excitation as a function of absorbed microwave power. Here we extend on the recent demonstration of SQUID-detected FMR [J. M. O'Reilly and P. Stamenov, Rev. Sci. Instrum. **89**, 044701 (2018)], of absolute scalar resonance measurements in single-crystalline and poly-crystalline YIG, at various fields and temperatures, by introducing a new set-up, where the microwave power, instead of being sunk in a matched load at the cryogenic end of the measurement probe is brought back to the ambient environment and is both metered and sunk in high dissipation power (>50 W @ 50 Ω) matching load. The here suggested methodology allows for the absolute excitation amplitude of modes excited during high-power operation of critical microwave devices, such as filters and Y-junction stripline circulators, to be predicted based on direct measurements of the same material in a known geometry.

## I. INTRODUCTION

SQUID-based ferromagnetic resonance (SFMR) detection has been recently showcased with measurements on poly-crystalline and single-crystalline yttrium iron garnet and shown to be capable of determining the absolute magnitude of the precession cone angle.[1] Within this technique, changes in the projection of the magnetisation along the applied field direction (the $z$-axis, as in Figure 1) are monitored using SQUID magnetometry as the material is driven into resonance. While this type of resonance detection (SFMR) is not explicitly sensitive to the phase of the precessing moment, with respect to the drive RF field, it can be co-located and in fact used concurrently (thus also providing phase information from conventional VNA-FMR) for the extraction of both the absolute absorbed power and the precession cone angle on resonance, which is typically a difficult task using conventional continuous-wave (CW) FMR. In the demonstration,[1] it is shown that the detected signal is quadratic as a function of the input RF power and the maximal power level is effectively directly limited by the allowed power dissipation at the 50 Ω termination at the end of the microstrip assembly carrying the sample, for the case, where only a single RF feed-line reaches the sample environment. Increasing the power brings quadratic gains in signal amplitude, but also brings about an increase in the extrinsic heating generated within the sample space. Here, it is shown that in order to circumvent this, a new reflection-transmission (return-track geometry) design can be constructed, using two parallel (cryogenic) RF-lines. Power can then be dissipated in a 50 Ω resistor externally, at ambient temperature, or for the case of VNA-FMR be connected to a secondary port, such that the two-port S-parameters can be determined. The knowledge of both the reflection and transmission coefficients allows for the quantitative extraction of the resonant absorption coefficients and thus the determination of the absolute magnetic
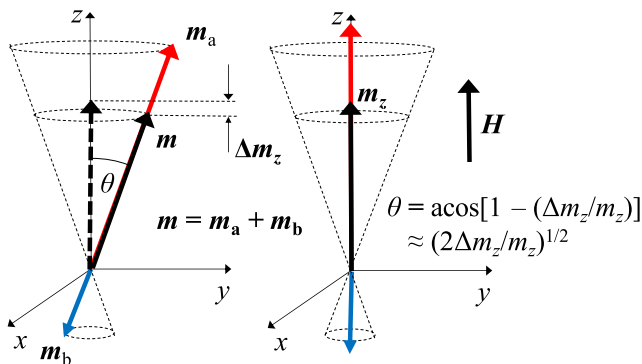
**FIG. 1**. Change in projection of the net magnetic moment along $z$ ($\Delta m_z$) during resonance, for a two sub-lattice ferrimagnet, within the macrospin approximation.

$$m = m_a + m_b$$

$$\theta = \mathrm{acos}[1 - (\Delta m_z/m_z)]$$
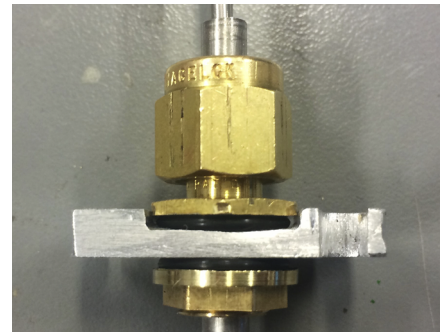$$\approx (2\Delta m_z/m_z)^{1/2}$$



**FIG. 2**. The Swagelock™-based clamp is fitted to the stainless steel shroud which is used to encapsulate the two coaxial lines. When hooked into the MPMS transport module, it allows motorized transport of the CPWs though the SQUID detection coils.

susceptibility (at RF and microwave frequencies), when operating at sufficiently low power levels, where $B_{RF} \ll B_{DC}$. In addition to this, external heat dissipation enables the measurement of ferromagnetic resonance at very high excitation power (in excess of tens or even hundreds of watts, provided that the sample absorption is low) and access to very non-linear dynamics, at large precession angles. The same is important, for example, for the definition of the fundamental limits of intermodulation distortion in critical high-performance microwave devices, such as filters and stripline circulators. Here, the apparatus is demonstrated in analysing the non-linear dynamics in a 1 mm diameter polished sphere of single-crystal yttrium iron garnet.

## II. EXPERIMENTAL

The new set-up contains many of the same features as the previous, such as the 8 mm diameter Cu shielding. However, the single coaxial line feeding into the microstrip transmission line is replaced by two semi-rigid coaxial lines feeding into either side of a double sided co-planar waveguide (i.e. two CPWs with a shared dielectric) carrier printed circuit board (PCB). The thickness of the dielectric ($t$=1.6 mm) is far greater than the pitch between signal and ground lines ($w$=0.3 mm) and hence is sufficient to avoid excessive cross-talk between lines, while still fitting within the 8 mm diameter shield. One side acts as the input port and the sample (YIG sphere) is fixed using varnish just to the side of the CPW's central conductor. The input CPW is then connected, at the end, to the opposing side, by a via (vertical interconnect access) to the secondary coaxial line. The two coaxial lines are held together using evenly spaced 4.6 mm diameter, 2 cm length stainless steal shrouds and Teflon washers to achieve the necessary level of mechanical rigidity and allow the rod to glide smoothly through the sample bore of the MPMS system. The top of the rod has a longer tube section, to which the sample transport sliding clamp is anchored. The Swagelock™-based clamp, as shown in Figure 2, was made to snugly fit the outer diameter of the stainless steel shroud.

The longer tube section is fitted with a custom-made 'slide-seal' vacuum assembly, fitting the corresponding receptacle of the Quantum-Design's stepper-motor-based transport load lock.[2,3] This assembly, when installed at the top of the sample transport

option provides a vacuum seal (including the differential pumping or helium flushing capability) while allowing the stainless steel rods to move vertically and the CPW to translate through the gradiometer coils. Figure 3 shows a schematic of the vacuum seal part, which consists of a chamber maintained using spring compression which divides two sealing sections. In Figure 3, parts 2 form an inner seal on the machined brass piece, while 3 are smaller rubber o-rings which form an outer seal on the stainless steal shroud used to house the two co-axial lines. All components are held within the brass piece using snap-ring compression. The standard Quantum-Design assemblies use a series of spacers and rubber lip-seals to maintain the chamber environment, in place of the spring compression design discussed here - a solution well-suited to small diameter sample rods. However, because of the larger access diameter required for the accommodation of the two RF lines, simple rubber seals would be more prone to degradation, both thermal and friction if the rod it not kept well lubricated with vacuum grease. When in operation, the fitting is continuously flushed with helium gas from the dewar via the two-ports on the brass piece, thus minimizing the amount of air pulled into the sample chamber as the rod moves through the seal. Having both the 'slide-seal,' assembly and the clamp to lock on to the transport motor means that it is possible to directly and concurrently
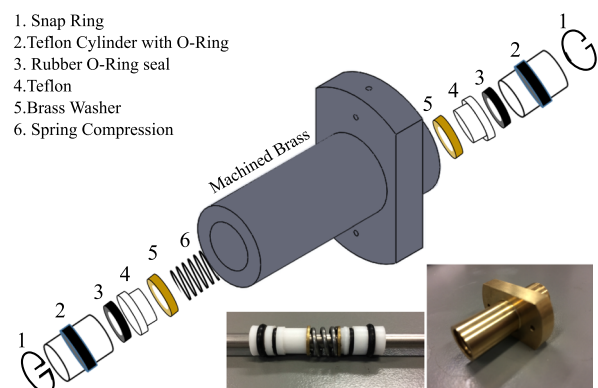
1. Snap Ring
2. Teflon Cylinder with O-Ring
3. Rubber O-Ring seal
4. Teflon
5. Brass Washer
6. Spring Compression



**FIG. 3**. Vacuum seal assembly for two port SQUID-FMR module.

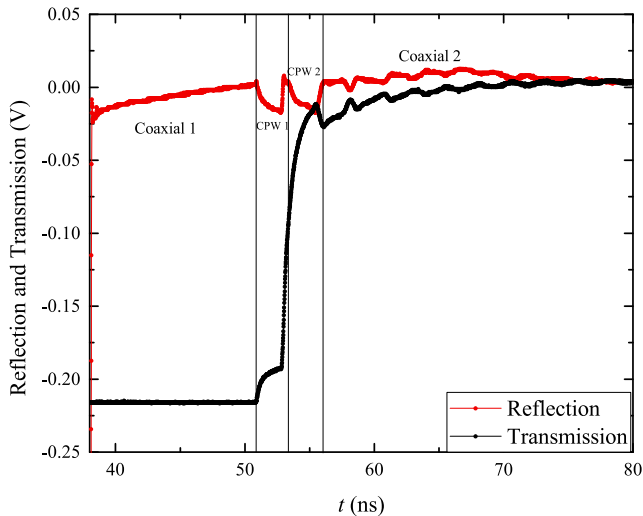**FIG. 4**. Complete return-track SFMR rod.



**FIG. 5**. TDR measured reflected and transmitted signals arising from the return-track set-up consisting of two CPWs and two co-axial feed lines.

perform DC and low-frequency AC magnetometry. The complete 'dual-port' assembly is shown in Figure 4.

Figure 5 shows the time-domain reflectometry (TDR), using reflected and transmitted signals through the entire RF circuit, where a fast edge pulse is launched into the SMA attached to one coaxial line and the transmitted signals are fed into the second TDR port through the SMA on the other line. Small losses are observed in coaxial 1 and coaxial 2, mostly due to their distributed resistance and their length. The two coplanar waveguides are labelled, as two well defined capacitive distortions to the incident signal. This is in part due to the small impedance mismatch to the CPWs, the abrupt discontinuities due to solder connections or vias and the finite capacitance to the outer RF shield.

## III. RESULTS AND DISCUSSION

The primary advantage of a two-port system is that it allows for higher input power and hence higher power absorption by the sample, which can greatly improve the sensitivity of the technique. This improvement is demonstrated in the automated sweeping of the athermally-detected SFMR spectra. Here the first module port provides 1 kHz chopped excitation signal to the sample via a 1-22 GHz signal generator and the second port feeds the transmitted signal into a 30 GHz bandwidth scalar spectrum analyser, such that the power dissipation can be monitored. The resonant response is monitored by the lock-in demodulated and processed SQUID voltage. A pulsed signal from a TTi arbitrary waveform generator provides synchronised triggering to both the signal generator (to initialise a linear frequency sweep) and to an oscilloscope connected to the

lock-in amplifier (to begin the trace). The digitized SQUID-response is then recorded through the common GPIB interface, using custom Labview software.

Some of the issues with the previous design are still unavoidable, for example, at specific frequencies resonant modes of the sample may couple strongly to the electromagnetic modes of the transmission lines and lead to distortion of the lineshape and in cases where the interference is constructive also lead to thermal propagation. At higher frequencies, in excess of 10 GHz, power delivery becomes an issue due to the dissipation and dispersion of the FR4 PCB board, which becomes highly lossy at high frequencies. Figure 6 shows the amplitude of the transmitted signal over the 22 GHz bandwidth, detected using the scalar spectrum analyser, which shows strong attenuation for frequencies in excess of 12 GHz and also high losses at specific frequencies corresponding to line resonances within the SFMR assembly. The material dispersion renders the periodicity of these variable. The coupling of FMR modes with line resonances, resulting in thermal propagation is depicted in Figure 7, where below 145 mT the amplitude of the primary mode increases significantly and the linewidth broadens and gains an asymmetric shape, characteristic of thermal dissipation. Thermal waves originating at the sample at the RF chopping frequency, propagate in the support structure and reflect at the transition to the RF feed-lines and at the bottom of the assembly. Any other dissipation, for example distributed losses in the CPW, also propagate through the structure and become significant at high power levels. The effect of these can be discriminated, based upon their dispersion, by varying the chopping frequency, as has been shown in Ref. 1. The details of the response depend on the level of thermal coupling between the sample and the assembly (contact area and thermal conductivity of the contact varnish) and level of coupling to the microwave transmission line resonances (which primarily depends upon the distance between the centre of the sphere and the highest magnetic field region above the CPW).
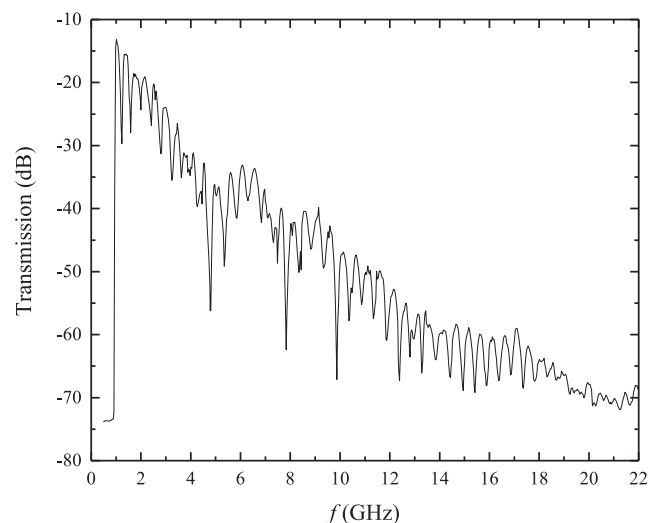


**FIG. 6**. The transmitted signal through the rod assembly shows strong attenuation beyond 10 GHz due to the dispersive nature of the FR4. In addition, losses occur at sharply defined frequencies corresponding to line resonances within the assembly.
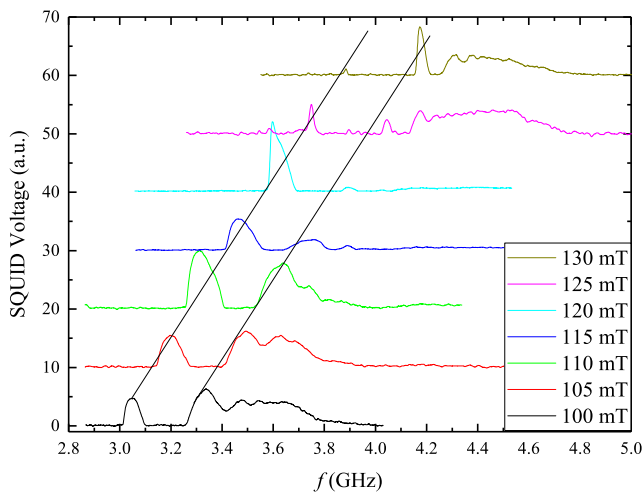
**FIG. 7**. Evolution of broad (thermal) resonances.

For applied fields $\mu_0 H$ in excess of 135 mT, multiple higher magnetostatic modes in addition to the primary mode are easily distinguished. These additional modes are only observable due to the non-uniform RF field distribution produced by the CPW and the enhanced power transmission and dissipation, made possible by the return-track assembly. Three of these higher modes are traced in Figure 8 but more may be seen at certain fields. The detectivity depends not only on the sample absorption and magnetic moment, but also on whether or not the resonance frequencies coinside with transission line resonances. Although the spatial positions of the magnetic field antinodes for these can be determined explicitly, here they are discriminated solely based on the fact that they do not disperse with the applied magnetic field. The traced magnetostatic
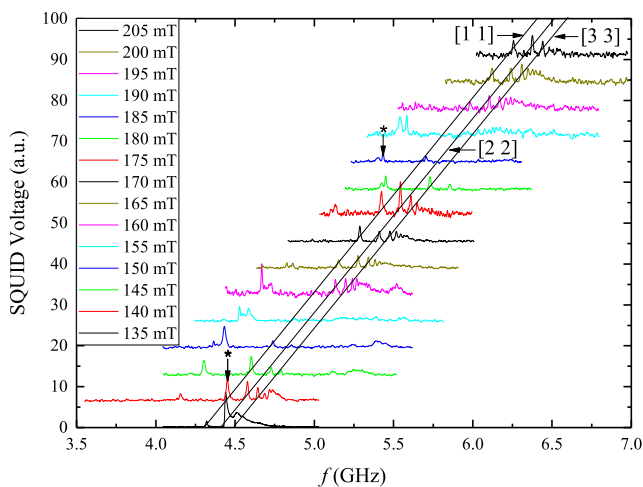


**FIG. 8**. At higher fields multiple distinct peaks that shift in frequency with changing field are observed, illustrating the detection of higher modes using automated athermal SQUID detection. The RF choping frequency is 1.23 kHz. The * denotes easily identifiable line resonances.
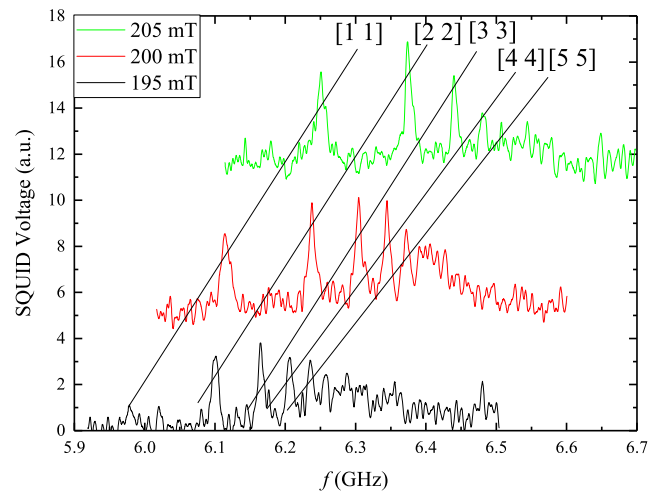


**FIG. 9**. Field dependence of the automatically scanned athermal SFMR spectra show tracking of higher order magnetostatic modes which appear to be more dispersive than the spatially uniform primary mode. The lines are simply guides to the eye. The RF chopping frequency if 1.23 kHz.

modes are indexed as [n m] following Walker.[4,5] For frequencies above 5.5 GHz, the amplitude of the transmitted power and hence the resonant response is diminished primarily due to microwave losses in the stainless steel coaxial lines.

Figure 9 shows a close examination of the evolution of the resonant peaks with increasing field strength. It appears that higher order modes are more field-dispersive than lower order ones (i.e. the separation between successive modes increases with the applied field). The fraction of the volume magnetisation of the sample, which is experiencing the higher affective anisotropy close to the surface of the sphere is increasing.

## IV. SUMMARY

A SQUID-magnetometry-detection, return-track geometry SFMR module is constructed and tested, which allows for power dissipation external to the cryogenic sample environment, thus lifting the previous limitation of 5 mW, dumped onto a cold 50 Ω terminator. This allows for greater excitation power and hence greater absorption by the sample, which significantly improves the absolute sensitivity of the technique (the same depends quadratically on the excitation power, for a fixed magnetic moment sensitivity). Automated frequency sweeping for the athermal SFMR for a single crystal YIG sphere is demonstrated. Multiple higher order modes, in addition to the uniform mode, are directly observable.

## ACKNOWLEDGMENTS

## REFERENCES

[1]J. M. O'Reilly and P. Stamenov, "SQUID-detected FMR: Resonance in single crystalline and polycrystalline yttrium iron garnet," Rev. Sci. Instrum. **89**, 044701 (2018).

[2]Quantum-Design, Magnetic Property Measurement System Hardware Reference Manual (2005).

[3]Quantum-Design, Slide Seal Assembly Rebuild; Service note 1014-602 Rev. A1.

[4]L. R. Walker, "Magnetostatic modes in ferromagnetic resonance," Phys. Rev. **105**, 390–399 (1957).

[5]N. J. Lambert, J. A. Haigh, and A. J. Ferguson, "Identification of spin wave modes in yttrium iron garnet strongly coupled to a co-axial cavity," J. Appl. Phys. **117**, 053910 (2015).